Available online at www.sciencedirect.com
SCIENCE DIRECT®
ELSEVIER
Nuclear Instruments and Methods in Physics Research A 531 (2004) 321–326
NUCLEAR INSTRUMENTS & METHODS IN PHYSICS RESEARCH Section A
www.elsevier.com/locate/nima

EXAFS study of mixed nickel molybdenum oxide thin films at the Ni and Mo K-edges

J. Gaidelene, R. Kalendarev, A. Kuzmin*, J. Purans

Institute of Solid State Physics, University of Latvia, Kengaraga street 8, LV-1063 Riga, Latvia

Available online 25 June 2004

Abstract

Mixed nickel molybdenum oxide thin films were produced by DC magnetron co-sputtering technique with the nickel content about 8, 16 and 25 at%. X-ray absorption spectroscopy at the Ni and Mo K-edges was used to study the local atomic structure in the films. The best-fit analysis of the EXAFS signals suggests that (i) the films are amorphous, except for the highest nickel content (25 at%), at which a segregation of NiO phase was observed; (ii) nickel and molybdenum atoms are octahedrally coordinated by oxygen atoms. Opposite to the NiO_6 octahedra, the MoO_6 octahedra are strongly distorted, that results in an existence of two groups of oxygen atoms—four nearest at $\sim$1.76 Å and two distant at $\sim$2.2 Å. It was also found that the MoO_6 octahedra are joined by edges, with the Mo–Mo distance about 3.26–3.31 Å.

PACS: 61.10.Ht; 78.70.Dm; 68.55.−a

Keywords: EXAFS; Ni K-edge; Mo K-edge; Nickel molybdenum oxide thin film

1. Introduction

Tungstates and molybdates have wide range of applications as phosphors ($CaWO_4$, $MgWO_4$) [1,2], scintillators ($ZnWO_4$, $CdWO_4$, $PbWO_4$) [1,2] and solid-state laser hosts ($CaW(Mo)O_4$, $SrW(Mo)O_4$, $PbMoO_4$) [3] when activated by rare-earth ions. Besides, $NiMoO_4$ is known among the most active and selective catalysts for oxidative dehydrogenation and selective oxidation of light hydrocarbons [4], whereas $NiWO_4$ exhibits electrochromic behaviour [5]. The optical and catalytic properties of these compounds depend strongly on the local coordination of W(Mo) ions, which is determined by the size of the cation [6]. For large cations such as Ca^{2+}, Ba^{2+}, Sr^{2+}, the scheelite-type structure with tetrahedral coordination of W(Mo) ions is adopted [6], whereas for small cations as Mg^{2+} and 3d ions from Mn^{2+} to Zn^{2+}, the structure is of wolframite-type with octahedral coordination of W(Mo) ions.

Our recent results for polycrystalline, nanocrystalline and amorphous $NiWO_4$ [5,7] have indicated that a decrease of the crystallites size influences strongly the local atomic and vibrational structures, leading to the preferential bonding of

*Corresponding author. Tel.: +371-725-1691; fax: +371-713-2778.
E-mail address: a.kuzmin@cfi.lu.lv (A. Kuzmin).

0168-9002/$ - see front matter © 2004 Elsevier B.V. All rights reserved.
doi:10.1016/j.nima.2004.06.023

tungsten ions to four oxygen atoms. At the same time, a change from tetrahedral to octahedral tungsten coordination occurs at high pressure in scheelite-type compounds [6,8]. Such interesting behaviour of tungstates stimulated further investigations for the case of molybdates. In particular, nickel–molybdenum oxide system will be discussed further.

Recently, the thin films of $NiMoO_4$ were produced by DC reactive sputtering [9]. According to X-ray diffraction (XRD) [9], the films deposited at substrate temperatures up to $T_s = 300^\circ C$ were amorphous, whereas a crystallization started at $T_s \sim 400^\circ C$ and polycrystalline α-$NiMoO_4$ structure with uniform sub-micron crystallites size was formed at $T_s \sim 525^\circ C$. The Raman study confirmed the presence of α-$NiMoO_4$ phase [9], whereas no other phase was observed by both XRD and Raman techniques [9]. Note that a formation of less stable high-temperature β-$NiMoO_4$ phase occurs in the bulk material at temperatures above $500^\circ C$ [10]. In α-$NiMoO_4$, both Ni and Mo atoms are octahedrally coordinated by oxygens, whereas in β-$NiMoO_4$ the coordination of Mo atoms changes to tetrahedral [10].

In this work, we present for the first time the X-ray absorption spectroscopy study of amorphous nickel molybdenum oxide thin films at the Ni and Mo K-edges.

2. Experimental and data analysis

Mixed nickel molybdenum oxide thin films were produced from nickel and molybdenum metallic targets by simultaneous reactive magnetron sputtering in a plasma-focusing DC magnetic field. A gas mixture of argon (70%) and oxygen (30%) was used as the sputter atmosphere. The sputter deposition was performed for 60 min at the total gas pressure 4–4.5 Pa. Glass and polyimide substrates were mounted about 8 cm above the target and were not intentionally heated. The films of several compositions were prepared. The Mo:Ni ratio was estimated from the values of the Ni and Mo X-ray absorption K-edges jumps. Three samples, considered below, had the following compositions: Mo:Ni = 75:25 for the sample A, 84:16 for the sample B and 92:8 for the sample C. The colour of the sample A was brownish, the sample B—light-brownish and the sample C—slightly brownish, nearly transparent.

Polycrystalline NiO [11] and pure molybdenum oxide thin films [12] were also used for comparison as reference compounds. Pure MoO_3 thin films were produced by thermal evaporation technique at different substrate temperatures T_s [12]. The amorphous thin film (a-MoO_3) was deposited at $T_s = 120^\circ C$, whereas polycrystalline thin films, having the phase of β-MoO_3 and α-MoO_3, were produced at $T_s = 300^\circ C$ and $345^\circ C$, respectively [12].

X-ray absorption spectra (XAS) at the Ni and Mo K-edges were recorded at room temperature using synchrotron radiation from the LURE DCI storage ring, operated at the energy 1.85 GeV and a maximum stored current 300 mA. A standard transmission scheme at the D21 (XAS-2) beamline, with a Si(3 1 1) double-crystal monochromator and two ion chambers containing nitrogen (I_0) and argon (I) gases, was used.

X-ray absorption spectra were analysed following conventional approach by the EDA software package [13,14]. The extended X-ray absorption fine structure (EXAFS) was singled out (Fig. 1) and best-fitted in the k-space range from 1 to 12 $Å^{-1}$ (Fig. 2) within multi-shell Gaussian/cumulant approximation [12,13,15]. The amplitude and scattering functions, required for the modelling, were calculated by the ab initio multiple-scattering (MS) FEFF8 code [16]. The FEFF8 calculations were performed at the Ni and Mo K-edges for two clusters of 8 Å radii, centred at the Ni and Mo atoms, respectively, and having α-$NiMoO_4$ structure [17]. The complex Hedin–Lundqvist exchange-correlation potential [18] was used to account for inelastic effects.

We have tried to find the simplest possible model with the smallest number of fitting parameters, which can adequately describe the experimental EXAFS signals. The structural parameters obtained from the best-fit analysis are given in Tables 1 and 2. Here the coordination numbers, related to the first coordination shell of Ni and Mo atoms, were first varied but were fixed in the final

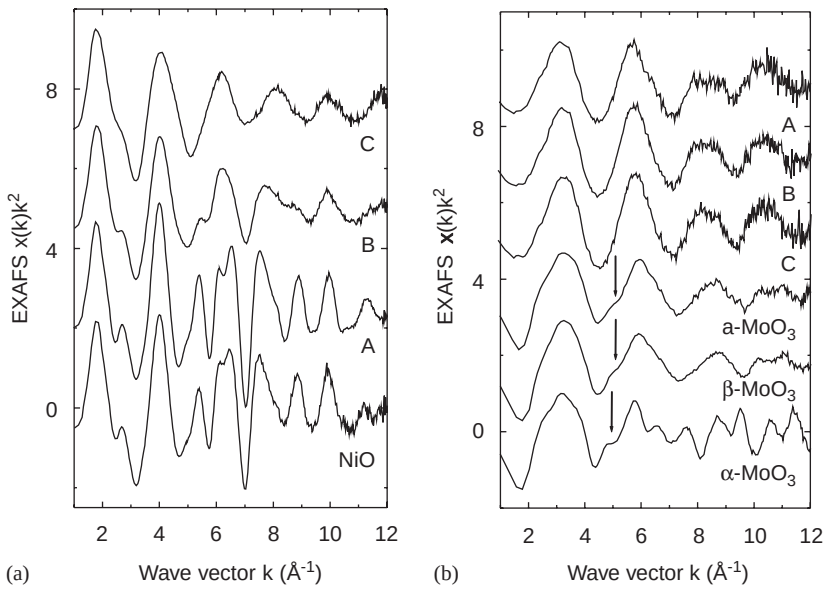

Fig. 1. (a) Experimental Ni K-edge EXAFS $\chi(k)k^2$ signals of mixed nickel–molybdenum oxide thin films (samples A, B, C) and polycrystalline NiO [11]. (b) Experimental Mo K-edge EXAFS $\chi(k)k^2$ signals of mixed nickel–molybdenum oxide thin films (samples A, B, C) and pure molybdenum oxide thin films (a-MoO_3, β-MoO_3, α-MoO_3) [12]. The shoulder, well visible at $k \approx 5\,\text{Å}^{-1}$ in pure molybdenum oxide thin films but absent in the mixed thin films, is indicated by arrows. The spectra are vertically shifted for clarity.

procedure at the found values to decrease the correlation between parameters and, thus, to increase stability of the fit. Note also that two multiple-scattering signals (MS)—double-scattering (DS) and triple-scattering (TS), generated within the first coordination shell of nickel ions were also required to explain the EXAFS signals for samples B and C (Table 1).

3. Results and discussion

The experimental EXAFS $\chi(k)k^2$ signals are of good quality with some noise present at high k-values (Fig. 1). Their Fourier transforms (FT) are shown in Fig. 2 and, except the data for Ni K-edge in sample C, consist of the two peaks. The main peak located at about 1.3–1.5 Å corresponds to the first coordination shell of Ni/Mo atoms, composed of oxygen atoms. The second peak at about 2.6 Å for the Ni K-edge and about 2.9 Å for the Mo K-edge is due to the next coordination shells (mainly the second shell) and multiple-scattering events within the first shell [19]. A set of peaks (Fig. 2), located at distances beyond 3 Å in the FT of the Ni K-edge EXAFS signal for sample A, indicates well-ordered local environment of nickel atoms. Note that the ordering around nickel atoms disappears for higher molybdenum content (samples B and C). The molybdenum environment is strongly disordered in all samples, so that already the second peak has enough small amplitude (Fig. 2). Note also that the absence of any peaks at long distances in FTs for the samples B, C and the sample A at the Mo K-edge suggests the statistical nature of the noise present in the experimental EXAFS signals in Fig. 1.

The qualitative comparison (Fig. 1) of the EXAFS signals for mixed nickel molybdenum oxide thin films and reference compounds allows us to make several conclusions. The sample A contains large amount of non-stoichiometric NiO phase, which is responsible for its brownish colour. The local environment around nickel atoms changes significantly in the samples B and C upon an increase of the molybdenum content. At the same time, the local environment of molybdenum atoms is rather similar in all samples but differs

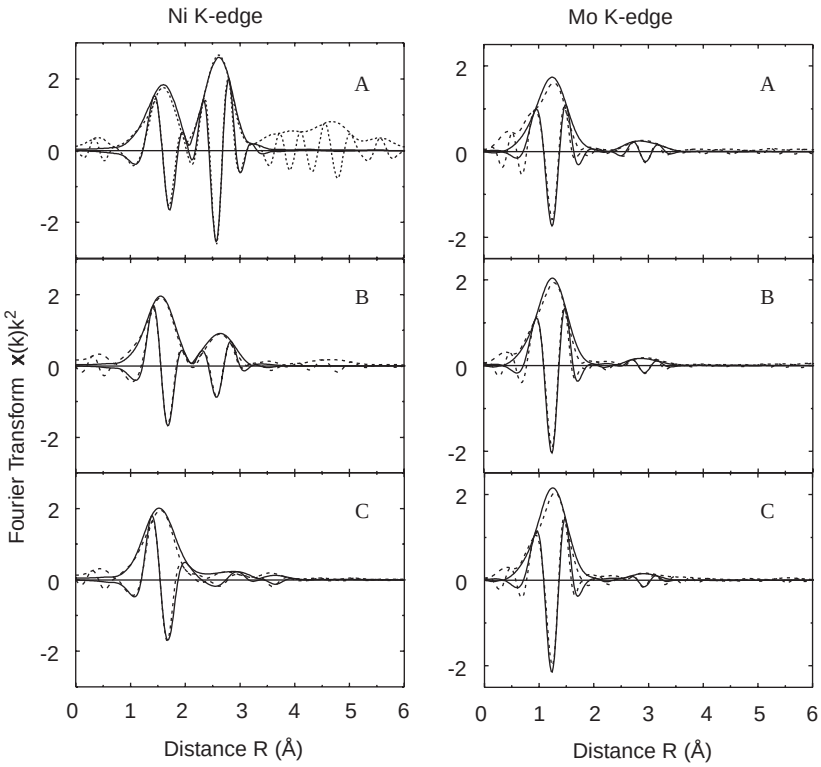

Fig. 2. Fourier transforms (FTs) of experimental (dash line) and calculated (solid line) EXAFS $\chi(k)k^2$ signals of mixed nickel–molybdenum oxide thin films (samples A, B, C). at the Ni (left column) and Mo (right column) K-edges. Note that FTs were not corrected for the scattering phase shifts, therefore positions of the peaks differ from true crystallographic values.

from that found in crystalline molybdenum oxide phases as α-MoO_3 and β-MoO_3 as well as in pure amorphous oxide a-MoO_3 [12]. As one can see in Fig. 1b, there is a characteristic shoulder at $k \approx 5\,\text{Å}^{-1}$ in all pure molybdenum oxide thin films. The absence of the shoulder in mixed nickel molybdenum oxides indicates a difference in the local environment of molybdenum atoms in pure and mixed molybdenum oxides at least beyond the first shell.

Further, we will discuss the quantitative results of the best-fit analysis, reported in Tables 1 and 2.

The changes in FTs at both the Ni and Mo K-edges (Fig. 2) upon an increase of molybdenum content indicate the loss of long-range order correlations, which can be induced by modification of the crystalline phase and a decrease of the crystallites size (amorphisation). The second coordination shell can be well observed in sample A around both Ni and Mo atoms and in the sample B around Ni atoms. It is only weakly observed around molybdenum in the samples B and C. No second shell signal was detected around nickel in the sample C, where two small peaks at 2.7 and 3.5 Å in Fig. 2 are, respectively, attributed to the multiple-scattering (DS and TS) signals, generated within NiO_6 octahedra [19]. The DS signal corresponds to the triangular scattering path $Ni_0 \rightarrow O_1 \rightarrow O_2 \rightarrow Ni_0$ with the angle $\angle O_1Ni_0O_2 = 90^\circ$. The TS signal corresponds to the linear scattering path $Ni_0 \rightarrow O_1 \rightarrow Ni_0 \rightarrow O_2 \rightarrow Ni_0$ with the angle $\angle O_1Ni_0O_2 = 180^\circ$. Here Ni_0 is the absorbing atom, and O_1 and O_2 correspond to two different oxygen atoms in the first shell.

Finally, one should note that at both edges no atoms of other type was detected in the second shell that indicates weak interaction between nickel and molybdenum sub-lattices.

Table 1
Structural parameters obtained from the multi-shell best-fit analysis of the Ni K-edge EXAFS spectra in mixed nickel–molybdenum oxide thin films

Sample	Shell	Amplitude	Distance R (Å)	Debye–Waller factor σ^2 (Å^2)	Cumulant C_3 (Å^3)	Fit error ε
A	O	6	2.08±0.01	0.010±0.001	—	0.09
	Ni	11±1	2.97±0.01	0.010±0.001	—	
	O	8	3.58±0.02	0.021±0.005	—	
B	O	6	2.06±0.01	0.009±0.001	—	0.04
	Ni	3±0.9	2.98±0.01	0.008±0.002	—	
	DS	24	3.47±0.02	0.0±0.007	—	
C	O	6	2.08±0.01	0.010±0.001	0.0011±0.0002	0.04
	DS	24	3.47±0.02	0.0±0.006	—	
	TS	6	4.05±0.03	0.015±0.007	—	

The amplitude means coordination number or multiple-scattering (DS and TS) path degeneracy; R is the interatomic distance or half-path length; σ^2 is the Debye–Waller factor; C_3 is the third-cumulant, indicating asymmetry of the distribution; ε is the fit error.

Table 2
Structural parameters obtained from the multi-shell best-fit analysis of the Mo K-edge EXAFS spectra in mixed nickel–molybdenum oxide thin films

Sample	Shell	Amplitude	Distance R (Å)	Debye–Waller factor σ^2 (Å^2)	Fit error ε
A	O	4	1.77±0.01	0.007±0.001	0.04
	O	2	2.20±0.02	0.020±0.004	
	Mo	1.5±1	3.26±0.02	0.009±0.006	
	O	2.5±1	3.51±0.03	0.006±0.006	
B	O	4	1.76±0.01	0.004±0.001	0.02
	O	2	2.21±0.02	0.024±0.004	
	Mo	1.4±1	3.26±0.02	0.012±0.005	
	O	3.6±2	3.46±0.05	0.025±0.025	
C	O	4	1.76±0.01	0.004±0.001	0.03
	O	2	2.23±0.02	0.025±0.004	
	Mo	0.4±0.4	3.31±0.07	0.005±0.007	
	O	1.8±1.0	3.38±0.04	0.007±0.017	

The amplitude means coordination number; R is the interatomic distance or half-path length; σ^2 is the Debye–Waller factor; ε is the fit error.

Similar situation was observed previously for nickel tungsten oxides [5,7].

In all three samples, nickel atoms have octahedral coordination by oxygen atoms, located at about 2.06–2.08 Å (Table 1). The distribution of the Ni–O distances is Gaussian-like in the samples A and B, however, becomes strongly asymmetric in the sample C, as indicated by the large value of C_3 cumulant. Molybdenum atoms are also octahedrally coordinated, but MoO_6 octahedra are strongly distorted with four short (1.76–1.77 Å) and two long (2.20–2.23 Å) Mo–O distances (Table 2). This suggests a displacement of molybdenum atoms in the direction of octahedra edges. From data in Table 2, one can estimate the average bonding angle $\angle Mo_0O_1Mo_2$ between two molybdenum atoms. From chemical point of view, two possibilities of connection between MoO_6 octahedra exist. In the first case, assuming $R_1(Mo_0–O_1) = 1.76$ Å, $R_2(Mo_2–O_1) = 2.23$ Å and

$R_3(Mo_1–Mo_2) = 3.31$ Å, the average bonding angle is about 111°. Whereas in the second case, assuming $R_1(Mo_0–O_1) = R_2(Mo_2–O_1) = 2.23$ Å, the average bonding angle is about 96°. Both results indicate that neighbouring MoO_6 octahedra are connected through the edge. Such local arrangement is different from that found in pure a-MoO_3 films, where oxygen polyhedra are connected by corners [12,20].

4. Conclusions

The local environment in mixed nickel molybdenum oxide thin films was studied by X-ray absorption spectroscopy at the Ni and Mo K-edges. The films were amorphous, except for high nickel content, at which a segregation of NiO phase was observed. In all films, both Ni and Mo atoms have octahedral coordination by oxygen atoms, and the interaction between nickel and molybdenum sub-lattices is very weak. Opposite to the NiO_6 octahedra, the MoO_6 octahedra are strongly distorted, so that one can distinguish two groups of oxygen atoms: four nearest O atoms are located at ~ 1.76 Å and are stronger bound to molybdenum atoms than two distant O atoms at ~ 2.2 Å. The estimate, based on the determined interatomic distances, suggests that MoO_6 octahedra are connected through edges. Such local environment is similar to that found in crystalline α-$NiMoO_4$ [17] and differs from that in pure molybdenum oxides [12].

Acknowledgements

This work was supported by the EC FP5 CAMART project and Latvian Government Grants 1.0811 and 1.0821.

References

[1] S.M. Gruner, M.W. Tate, E.F. Eikenberry, Rev. Sci. Instrum. 73 (2002) 2815.
[2] V.N. Kolobanov, et al., Nucl. Instr. and Meth. A 486 (2002) 496.
[3] A.A. Kaminskii, Laser Crystals, Springer, Berlin, 1981.
[4] C. Mazzocchia, C. Aboumrad, C. Diagne, E. Tempesti, J.M. Herrmann, G. Thomas, Catal. Lett. 10 (1991) 181.
[5] A. Kuzmin, J. Purans, R. Kalendarev, D. Pailharey, Y. Mathey, Electrochim. Acta 46 (2001) 2233.
[6] A.W. Sleight, Acta Cryst. B 28 (1972) 2899.
[7] A. Kuzmin, J. Purans, R. Kalendarev, Ferroelectrics 258 (2001) 21.
[8] A. Kuzmin, et al., Physica Scripta (2004), in press.
[9] J.Y. Zou, G.L. Schrader, Thin Solid Films 324 (1998) 52.
[10] J.A. Rodriguez, J.C. Hanson, S. Chaturvedi, A. Maiti, J.L. Brito, J. Chem. Phys. 112 (2000) 935.
[11] A. Kuzmin, J. Purans, A. Rodionov, J. Phys.: Condens. Matter 9 (1997) 6979.
[12] A. Kuzmin, J. Purans, Proc. SPIE 2968 (1997) 180.
[13] A. Kuzmin, Physica B 208&209 (1995) 175;
A. Kuzmin, J. Physique IV (France) 7 (1997) C2–213.
[14] A. Kuzmin, J. Purans, J. Phys.: Condens. Matter 12 (2000) 1959.
[15] V.L. Aksenov, A.Y. Kuzmin, J. Purans, S.I. Tyutyunnikov, Phys. Part. Nucl. 32 (2001) 675.
[16] A.L. Ankudinov, B. Ravel, J.J. Rehr, S.D. Conradson, Phys. Rev. B 58 (1998) 7565.
[17] H. Ehrenberg, et al., J. Magn. Magn. Mater. 150 (1995) 371.
[18] J.J. Rehr, J. Mustre de Leon, S.I. Zabinsky, R.C. Albers, J. Am. Chem. Soc. 113 (1991) 5135;
J. Mustre de Leon, J.J. Rehr, S.I. Zabinsky, R.C. Albers, Phys. Rev. B 44 (1991) 4146.
[19] A. Kuzmin, R. Grisenti, Philos. Mag. B 70 (1994) 1161.
[20] A. Balerna, et al., Nucl. Instrum. and Meth. A 308 (1991) 234.